

Experimental and Numerical study of (CH₃NH₃PbI₃) MAPbI₃ thin film with fluorene- dithiophene (FDT) or spiroometad as hole transporter layer

ABOUbakarycoulibaly^{*1,3,4}, Amal Bouich^{1,2}, Shafi ullah¹,
N'guessanRaymond Kre³, Boko Aka^{3,4}, Bernabé Mari¹

¹Institut de Disseny i Fabricació, Universitat Politècnica, València, Spain

²Laboratoire (LMEE)-Ibn Tofail university of Kenitra, Morocco

³Université Nangui Abrogoua, UFR des Sciences Fondamentales et Appliquées (SFA), Abidjan, Côte d'Ivoire

⁴Institut de Recherche sur les Energies Nouvelles (IREN), Abidjan, Côte d'Ivoire

Abstract: Here, we have investigated the organic-inorganic CH₃NH₃PbI₃(MAPbI₃) thin films. We performed the x-ray diffraction, SEM and AFM, to control the Crystallinity, Thickness, Transmittance and Absorption of the thin films. Then the photoluminescence was studied to know the band gap of the material. The simulation was carried out on the cell formed of organic-inorganic perovskite MAPbI₃ thin film as absorber layer with different hole transporter layer, expensive Spiroometad or cheaper FDT, ZnO as electron transporter material (ETM). The comparison performance was made between the cell with spiroometad and the cell with FDT. The spiroometad and FDT cells displayed a similar efficiency of 23.4% after simulation.

Keys words: MAPbI₃, XRD, simulation, HTM, spiroometad, FDT, efficiency.

Date of Submission: 17-03-2020

Date of Acceptance: 02-04-2020

I. Introduction

Since the discovery of semiconductor properties of the hybrid organic-inorganic halide perovskites in 2009 by T. MIYASAKA [1] these materials have become star of research in laboratories and conferences. Used as an absorber layer in a solar cell, this material initially showed a low conversion efficiency of 3.5% in 2009. So researchers have objective to improve performance and nowadays we achieve efficiency at 25.3% for a perovskite solar cell [2]. Halide perovskite materials have good properties that open door to a new generation of photovoltaic cells [2]. The real perovskite is a mineral found for the first time in 1839 on the Ural Mountains, composed of a calcium and titanium oxide (CaTiO₃), named after the Russian mineralogist Lev Perovskite [3,4]. This name has subsequently become synonymous with all compounds that have the same crystallographic structure of the mineral: ABX₃ where A⁺ is a monovalent cation in the center of a cube, B²⁺ are divalent cations placed at the top of the cube and X⁻ smaller anion monovalent on the faces of the cube and which compose octahedral structures where B on each vertex of the cube. Depending on the type of atoms or molecules chosen, it is possible to obtain materials with particular characteristics and very interesting for the conversion of energy. In the case of perovskite solar cells, the most perovskite compound have being obtained the best results is the lead and methylammonium trihalide of formula (MAPbX₃), characterized by a direct band gap between 1.5eV to 2.3 eV, capable of providing high energy efficiency [5, 6]. The toxicity of lead has led to study perovskites based on other ions such as (CH₃NH₃SnI₃) which have a band gap of 1.3 eV but this perovskite suffers from stability due to the oxidation of the ion Sn²⁺ to Sn⁴⁺[7].

The simplicity of the manufacturing technique and the combination of the relevant properties, such as excellent optical and electrical properties, including the high absorption coefficient [8], ideal gap bands [9], low exciton bonding energies [10] transport of ambipolar charge carriers [11] and long charge diffusion lengths [12] make the perovskite structure highly competitive characteristics compared with conventional semiconductors. To change from the status of a star research object to a marketable industrial product, perovskite solar cells have to be proved in terms of efficiency and stability and low cost of production soaring [13]. In a perovskite solar cell there is perovskite layer between a hole transport material (HTM) layer and an electron transport material (ETM) layer. Perovskite is the active layer where the electron-hole pairs or excitons are photogenerated. After the dissociation of the excitons, the electrons are transferred to ETM and the holes to HTM. The cell efficiency depends on the choice of these two layers: ETM and HTM. ETMs are easily found cheaper and compatible with perovskite MAPI giving good performance but this is not the case with HTMs.

Various materials inorganics [14, 15] as organics [16], are used as HTM in perovskite solar cells. The semi-conductor material that gives the best efficiency is the organic compound 2,2',7,7'-tetrakis (N, N-dip-p-

methoxyphenyl-amine)-9,9'-spirobifluorene (spiro-MeOTAD)(figure 1b1). Unfortunately, its synthesis is very expensive [17]. Research is always done to find the material capable of replacing spiroometad with a low cost of synthesis and keeping the same performance. In 2015 Prof.Mohammad KhajaNazeeruddin and coworkers [18]have developed a new hole transporter material for solar cells, which significantly reduces manufacturing costs and achieves a very competitive efficiency of more than 20%. The new molecule is fluorene-dithiophene (FDT) with chemical name 2,7-bis(4-methoxyphenyl)amino)spiro[cyclopenta[2,1-b:3,4-b]dithiophene-4,9-fluorene)(figure1b2)[18]. Extensive testing has shown that the FDT's efficiency is 20.2%, which is higher than the other two more expensive products (Spiro ometad and PTAA) [19]. Even better, the FDT's features are easy to modify, so it can serve as the basis for a whole new generation of more economical hole transporters (HTM) [19].

II. Experimental procedure

We used the FTO glass substrate for the deposition of absorbent layer perovskite of our solar cell. This FTO glass substrate was subjected to an ultrasonic bath in soapy water (2% Hellmanex); in ethanol; in acetone and then in isopropanol for fifteen minutes at each stage. All these products were purchased from TCI. Afterwards the glass substrate is dried by an air tap and then subjected to a UV-ozone treatment for fifteen minutes. All these steps must be scrupulously respected without neglecting anything because the quality of the films depends on it. Studies have shown that FTO substrates without UV-ozone-treatment of films are of low quality in thickness and morphology.

- **Synthesis of CH₃NH₃PbI₃ (MAPI) solution**

The precursors are methylammonium iodide (MAI) (99.99%; TCI) and lead diiodide (PbI₂) (99.99%, TCI). These crystals are weighed and dissolved in a mixture of solvents: dimethylsulfoxide (DMSO) and dimethylformamide (DMF) (ratio 0.095:1). We obtain a MAPI solution of 1.35M. We can accelerate the dissolution of PbI₂ by heating to 60 °C.

- **Deposition of thin film of perovskite**

Among the many deposition techniques we preferred the spin coating deposition which is the most simple and easy. First we set the spin coating at different speeds with different times. We made the deposit before the rotation of the spinner (static deposition) and the deposit during the rotation of the spinner (dynamic deposition). The best results are obtained with the static deposition by maintaining an acceleration speed from 2000rpm to 6 s and the second speed at 6000 rpm for 60 s. So a volume of 50μL of perovskite solution is taken and applied to the FTO part of the substrate, then the spinner is started. A volume of 50μL chlorobenzene playing the role of anti-solvent is applied to the perovskite when there is a change in color. The time of application of the anti-solvent is around 10s to 15s. Then the samples are annealed at a temperature of 85 °C for 5 min. The samples are immediately placed in the dark for characterization. We carried out all these experiments outside glovebox at room temperature.

- **Characterization**

X-ray diffractometer(RIGAKU) was used for structural characterization. Also, Scanning ElectronMicroscopy (SEM) was used to investigate the surface morphology,Atomic force microscopy(AFM) for topography, Photoluminescence (PL) and UV-Vis spectroscopy. X-ray diffraction spectrum of a MAPbI₃ powder having a single phase of tetragonal symmetry at room temperature [20] .In the X-ray diffraction (XRD) patterns of MAPbI₃ shown in figure 1.a, the peaks are at 14.06° and 31.89° belong to perovskite structures and are in good agreement with recent reports. The photoluminescence of the MaPbI₃ show intense peak after annealing procedure and shown characteristic peak of MaPbI₃at 774nm, we also found that the good absorption onset at a 426 nm. The calculation of the energy of optical gap gave a value of E_g equal to 1.5eV (figure 1-e); value close to the literature. Figure.2 represent the SEM and AFM images of MAPbI₃. MAPbI₃ has an improved thin film formation with smaller grain size and surface show homogenous and smooth morphology.

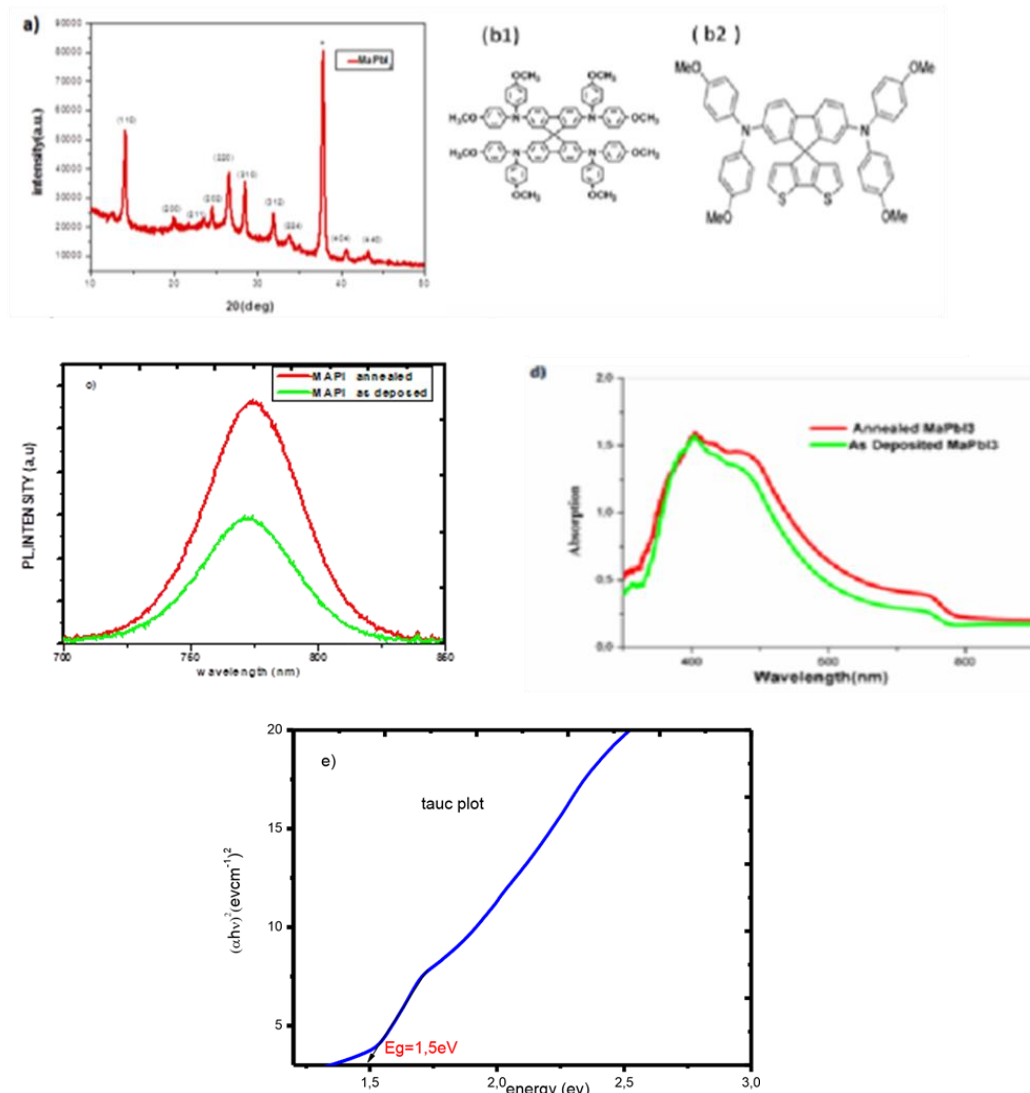


Figure 1: (a) xrd patterns of $MAPbI_3$; (b) molecular of spiro ométad; (b2) molecular FDT; (c) PL of $MAPbI_3$ (d) absorption of $MAPbI_3$; (e) band gap of $MAPbI_3$.

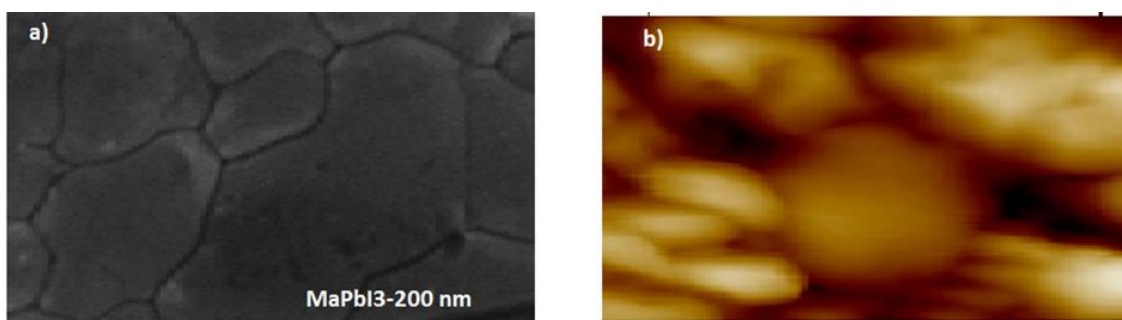


Figure 2: a) SEM image of $MaPbI_3$ thin film b) AFM image of $MaPbI_3$ thin film obtained

III. Numerical Modelling and Device Simulation.

3.1 Numerical Modelling

Numerical simulation is used to investigate the effect of the different layer components on the performance of perovskite solar cells without actually making the device. It saves time and money in the search for the best experimental results. Many simulation software programs have been developed and applied to research solar cell devices such as AMPS-1D, SCAPS-1D, PC1D, AFORS-HET and so on. All these programs are at a single dimension, which is usually sufficient for geometry solar cells. We choose SCAPS-1D who is a

one-dimensional solar cell simulation program developed at the department of Electronics and Information Systems (ELIS) of the University of Gent, Belgium by prof. Marc Burgelman. It simulates the electrical characteristics of heterojunction thin-film solar cells by solving the basic equations of semiconductor devices under steady state conditions. It is used in this work to explore the real device solar cell with material parameters modified for better performance. SCAPS-1D allows the inclusion of deep recombination and recombination (non-radiative recombination). Here the basic equations of semiconductor devices.

• **Poisson’s equation**

The best understanding of the working of a solar cell is governed by the resolution of the Poisson’s equations; equations of continuity and equations of transport of electrons and holes in the cell. The Poisson’s equation allows for a relationship between the variations of the potential electrostatic and the density of electrical charge. [21]

$$\frac{\partial^2(\varphi)}{\partial x^2} = -\frac{\rho(x)}{\epsilon_r} = -\frac{q}{\epsilon_r} (p - n + N_d^+ - N_a^-) \text{ (eq.1)}$$

φ is the electrostatic potential, n and p the concentrations of electrons and holes, N_d⁺-N_a⁻ is the impurity concentration, ε_r is the relative dielectric constant of perovskite.

• **Continuity equation**

In order to establish the variation of the concentrations of the charge carriers at a point x of the cell; we define the continuity equation whose expression is:

$$\frac{\partial n}{\partial t} = -\frac{\partial J_n}{\partial x} + G_n - R_n \text{ (eq.2)}$$

$$\frac{\partial p}{\partial t} = -\frac{\partial J_p}{\partial x} + G_p - R_p \text{ (eq.3)}$$

G_{n,p} are generation rates of electrons and holes and R_{n,p} are recombination rates of electrons and holes in the device.

• **Transport equation**

To solve these equations, the knowledge of generation and current recombination mechanisms is necessary. The currents of electrons and holes result from the sum of two factors: a gradient of electrostatic potential and a gradient of concentration. [21]

$$J_n = qn\mu_n \frac{\partial V}{\partial x} - D_n \frac{\partial n}{\partial x} \text{ (eq.4)}$$

$$J_p = qp\mu_p \frac{\partial V}{\partial x} + D_p \frac{\partial p}{\partial x} \text{ (eq.5)}$$

With μ_n and μ_p which represent the mobilities of electrons and holes, n and p the density of holes and free electrons; D_n (D_p) is electron (hole) diffusion.

3.2 Device Structure and Simulation

3.2.1 Device Structure

In general, the architecture of the perovskite solar cell consists of five layers: a transparent electrode, an n-type semiconducting electron transporting material (ETM), photoactive perovskite, a p-type semiconducting hole transporting material (HTM) and a metallic electrode (figure 3 (a)). The parameters of TCO and HTM layers are cited from the simulation literature about PSCs. Note that the main material parameters are carefully selected from those reported experimental data and other theoretical results. Tables 1,2 summarize the parameters for each layer in the simulation and their interface defect properties.

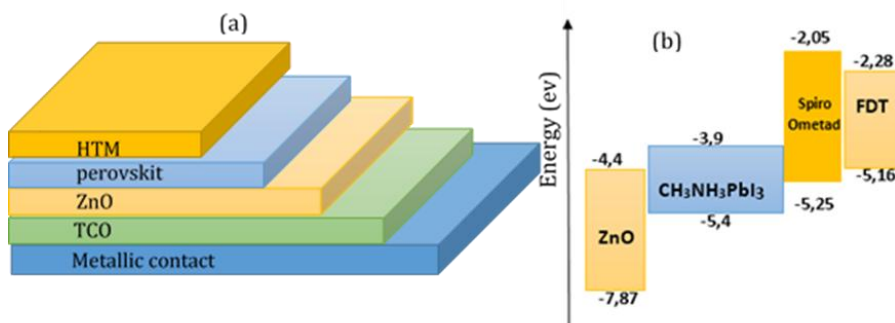


Figure 3: (a) Schematic structure of the device (b) energy band

Table 1: Simulation parameters of perovskite solar cells

Material Properties	MAPI	Spiro-OMETAD	FDT	ZnO	TCO
X (μm)	varied	0.05	0.05	0.03	0.5
E _g (eV)	1.5	3.0 [23]	2.88[36]	3.3[25]	3.5 [25]
χ (eV)	3.9 [26]	2.45 [23]	2.28[36]	4.4 [25]	4 [25]
ε _r	6.5 [27]	3 [23]	5	9 [25]	9 [25]
N _c (cm ⁻³)	2.10 ¹⁸	2 × 10 ¹⁸ [22]	10 ¹⁹	2 × 10 ¹⁸	2 × 10 ¹⁸
N _v (cm ⁻³)	10 ¹⁹	10 ¹⁹	10 ¹⁹	10 ¹⁹	1.8 × 10 ¹⁸
v _n (cm.s ⁻¹)	10 ⁷	10 ⁷	10 ⁷	10 ⁷	10 ⁷
v _p (cms ⁻¹)	10 ⁷	10 ⁷	10 ⁷	10 ⁷	10 ⁷
μ _n /μ _p (cm ² /v.s)	2.0/2.0 [28]	2.10 ⁴ /2.10 ⁴ [27]	5.10 ⁻⁴ /5.10 ⁻³	20/10 [25]	20/10 [25]
N _d (cm ⁻³)	varied	0	0	10 ¹⁶	2.10 ¹⁹
N _a (cm ⁻³)	0	10 ¹⁸	10 ¹⁸	0	0
N _i (cm ⁻³)	10 ¹⁴	10 ¹⁴	10 ¹⁴	10 ¹⁴	10 ¹⁴
E _i (eV)/ distribution	0.7 ev above eV	0.1 ev above eV	0.7ev above eV	0.6ev above eV	0.6ev above eV

Table2: Interface defect properties panel

Defect type	Neutral
capture cross section electron(cm2)	1.000-15 [29]
capture cross section hole(cm2)	1.000-15 [29]
Energetic distribution	single
Reference for defect energy level Et	Above the highest EV
Energy level with respect to Reference (ev)	0.600
Total density(integrated over all energies)(cm ⁻²)	1.000E+14

3.2.2Simulation

• Effect of Thickness of the perovskite Layer

For commercial production on large surfaces and in large quantities, the reduction of manufacturing costs is essential. The reduction of the thickness of the absorbent layer is a desired factor in order to use less material without reducing the performance of the solar cell. Thus, it is important to study the influence of the layer thickness on the output parameters of the solar cell namely the efficiency, the open circuit voltage, the fill factor, the current density. We present the results of our simulations in Figure 4 to understand how the variation in layer thickness influences the characteristics of the cell.

By observing the variation curves of the thickness of the perovskite layer in fig. 4, an increase in the Voc, Jsc and PCE parameters is observed. On the other hand, the fill factor (FF) decreases using FDT. Thus, for thickness values ranging from 100 nm to 400 nm, there is an increase of PCE to 37% for MAPI-FDT cell and 63% for MAPI-Spiro Ometad cell. When we increase the thickness beyond 400 nm, there is a slight increase in current density of less than 5% for all the cells studied. As for the value of the voltage (Voc), it increases very slightly less than 1% for all the cells. The Voc of spiroometad are larger than those of FDT, at 600nm, we have 1.01v and 0.86V respectively for the spiroometad and the FDT. Regarding the fill factor (fig 4-c) there is a drop of about 4% for MAPI-FDT and increase of 8% for MAPI-spiroometad cell. It can be seen that increasing the thickness from 100 nm to 400 nm increases the PCE to 75% and 27% for MAPI-spiro and MAPI-FDT cells respectively. The MAPI associated with spiroometad confirms its properties of better perovskite converter solar energy [25] with PCE = 19.22% at 350 nm against 18.63% if it is associated with the FDT. Beyond 400 nm the efficiencies increase very slightly around 5% to 8% for the cells. At a thickness of 600 nm, the efficiency is 20.6% with MAPI-FDT, 21.35% with MAPI-Spiro ometad. The variation of the thickness of the absorber layer from 100 nm to 400 nm causes a significant increase in the parameters of the cells. This is normal because a thicker layer absorbs more photons. Beyond 400nm, the efficiency increases slightly because there is appearance of the defects. When the diffusion length of the charge carriers becomes greater than the thickness, many of them recombine and are not collected. This explains the weakness of the increase of the parameters of the cells beyond 400nm.

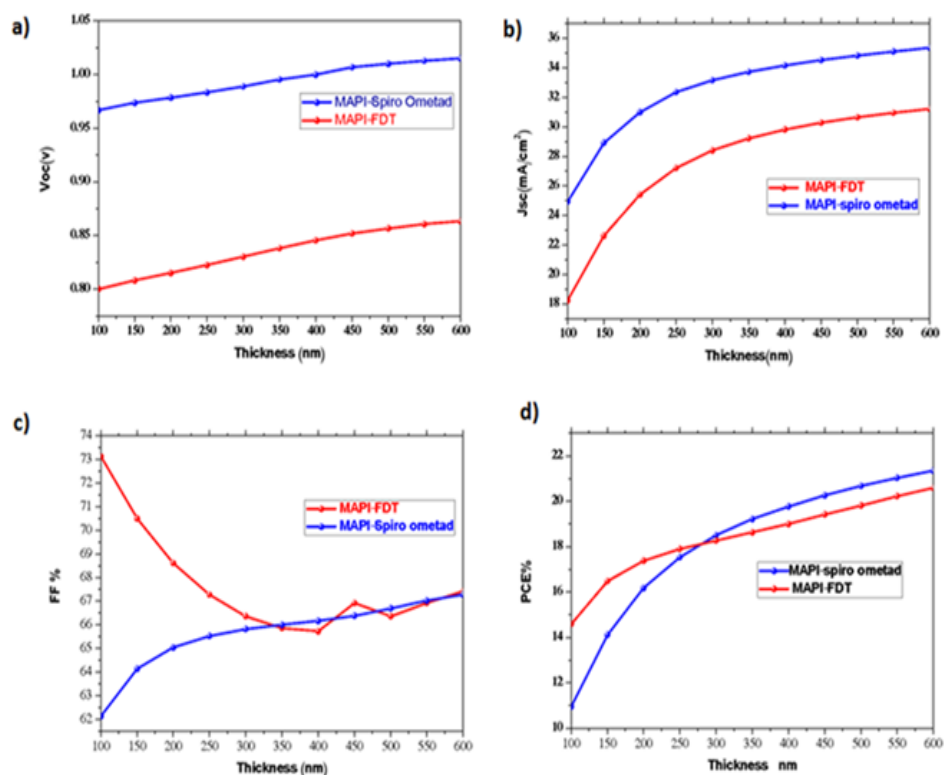


Figure 4: variation Voc (a) Jsc (b) FF(c) and PCE (d) with different thickness of perovskite

- **Effect of doping concentration of perovskite absorption layer**

The effect of doping concentration on the performance of perovskite solar cells is studied by choosing the values of Na in the range of 10^{12} to 10^{18} cm^{-3} . It is worth pointing out that the variation of the doping concentration of perovskites modifies all parameters of the cell. The figure 5-d delivers the PCE of solar cells. The maximum values of PCE appears at $Na=10^{16}$ cm^{-3} for all the cells with 21.13% for FDT and 21.04% for spiroometad. There is a slight variation of efficiencies when the concentration varies from 10^{12} to 10^{14} cm^{-3} . Beyond 10^{14} cm^{-3} to 10^{16} cm^{-3} , efficiencies suddenly increase to 16.93% to 21.13% for FDT and 17.05% to 21.04% for spiroometad to reach maximum values at 10^{16} cm^{-3} then they decrease after this value. On the other hand, the Jsc (fig5-b) and Voc (fig5-a) parameters adopt similar behaviors to that of efficiencies. From 10^{12} cm^{-3} to 10^{16} cm^{-3} the current density remains almost constant after Jsc drops rapidly. The optimum values of Jsc are 29.67 mA/cm^2 and 33.74 mA/cm^2 for spiroometad and FDT respectively. As for the Voc the maximum values are obtained at 10^{15} cm^{-3} (Voc= 0.99v) for spiroometad and at 10^{17} cm^{-3} (Voc=0.86v) for the FDT. Doping is a very important process used to improve optoelectronic properties of semi-conductors [19]. It is possible to improve the conductivity of the hole transporter layer by doping the perovskite absorber therefore improves the performance of the cell [20]. The justification of the variation of cell performance by doping concentration is that the electrical field in the semiconductor varies when the concentration varies. When we increase the concentration and the parameters of the cell remain, almost constant this means that the recombination defects appeared have annihilated the carriers brought. At a certain value of the concentration, the photogenerated carriers dominate the recombination then the efficiency and the other parameters increase to reach an optimal value. If the concentration is further increased, the recombination rate increases again causing the efficiency to fall as shown in Fig. 5-d. The results of simulations show that the cell with the FDT has a simulated behavior to that of spiroometad.

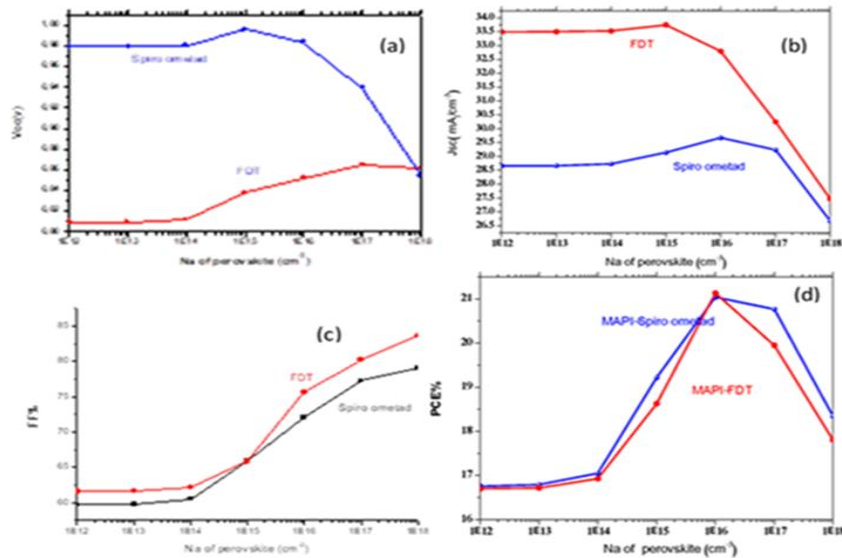


figure 5 : variation Voc (a) Jsc (b) FF(c) and PCE (d) with concentration of perovskite

• **Influence of doping concentration (Na) of HTM**

Appropriate doping of the HTM layer increases the electric field of the interface HTM / perovskite and improves the performance of the cell. To understand the doping effect of the HTM on the cell performance, the concentration Na of the HTMs vary to 10¹² at 10²² cm⁻³. This increase electric potential used to separate the excitons with less recombination rate so the performance of the device is increased.

From the graph figure 5 concentration acceptor (Na) versus PV parameters, it was observed that Voc, FF, Jsc, efficiency have been increasing, with an increase Na of HTM. It indicates that the spiroometad is shown to have a higher Voc (1.02V) than the FDT (Voc=0.88V) while the FDT has a Jsc (34 mA/cm²) greater than the spiroometad (Jsc=30mA/cm²). Curves (c) and (d) indicate that the two HTMs give the same value of FF = 76% at 10²¹ cm⁻³ and the identical efficiency PCE = 23.4% at 10²² cm⁻³.

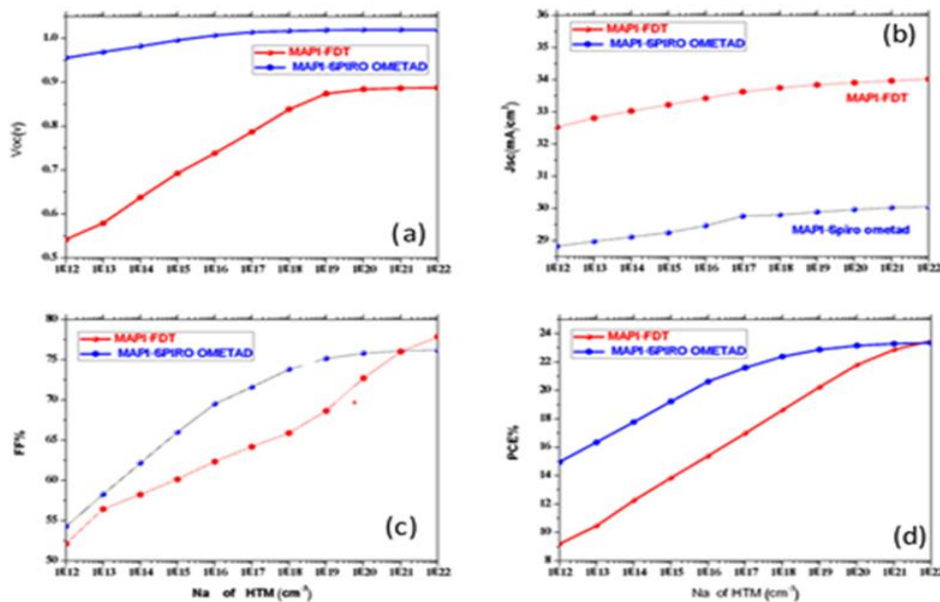


Figure6:variation Voc (a) Jsc (b) FF(c) and PCE (d) with different concentration Na of HTM

• **Influence of electron affinity of perovskite absorber layer and HTMs layers**

One of the decisive factors of carrier recombination at interface is the band offset between ETM/perovskite/HTM which determines the parameters of cell [30]. Electronic affinity is defined as the energy that must be supplied to an electron located in the bottom of the conduction band CB to bring it to the vacuum

level. As seen in Figure 7 all the parameters of the cell are modified with the variation of the electronic affinity of the HTMs. The simulation results indicate that the Spiroometad gives a $V_{oc}=1.02v$ and the FDT has $V_{oc}=0.88v$. The cell with FDT has a higher current density ($J_{sc}=34mA/cm^2$) than that of Spiro ometad ($J_{sc}=30mA/cm^2$). The fill factor curves and efficiencies are almost similar with a slight domination of FF and PCE of FDT (FF= 78.8% and PCE =23.82%) to that of Spiroometad (FF= 76% and PCE= 23.18%).

When the electron affinity of HTM is too low (lower than 2.4 eV), the parameters V_{oc} , FF, PCE are a bit weak. The value of the current density varies very little during the variation of the electronic affinity from 2ev to 3ev. After the value of 2.4ev we obtain an optimal value of V_{oc} for each HTM. At the value of 2.5 ev the parameters FF and PCE reach the optimal values. It is evident that proper HTM selection with suitable electron affinity can reduce the recombination of carriers and performance of PSCs can further be optimised [23].

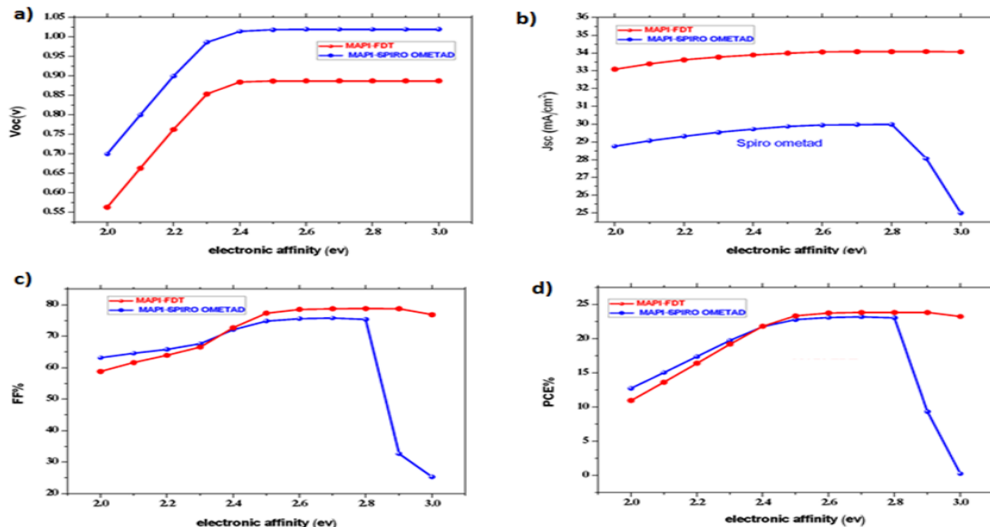


Figure 7: variation V_{oc} (a) J_{sc} (b) FF(c) and PCE (d) with electronic affinity of perovskite

• Curves J-V and External Quantum Efficiency(EQE)

EQE (Extern Quantum Efficiency EQE) refers to the fraction incident photons that creates the pairs electron-hole in the absorber and are collected. EQE is a parameter used to characterize a photosensitive component such as a photovoltaic cell. It provides information on the quality of the materials and contacts used in the cell [31]. To obtain the final curve J-V, we kept all optimal values of the parameters of the cell. The simulated J-V and EQE curves are shown in Figure 8 below. The optimal parameters are for the cells : thickness of perovskite (500nm), doping concentration of perovskite ($10^{16}cm^{-3}$), doping concentration of HTM ($10^{21}cm^{-3}$), electronic affinity of HTM (2.8 ev). The final model displays the voltage $V_{oc} = 0.88v$ for the FDT and $V_{oc} = 1.02v$ for the Spiroometad (Fig.8a). It is indicated at figure 8b that the EQE increases slowly from wavelength 300 nm until around 350 nm for FDT and 400nm for Spiro ometad, then remains in a relatively steady high position until wavelength 850 nm, before dropping to 1000 nm. The maximum EQE value is 73.02% for FDT and 86.37% for Spiroometad. From 850 nm, the EQE is low because the corresponding energy is lower than the energy band gap of perovskite. Any light with energy below the band gap will not be absorbed by the cells.

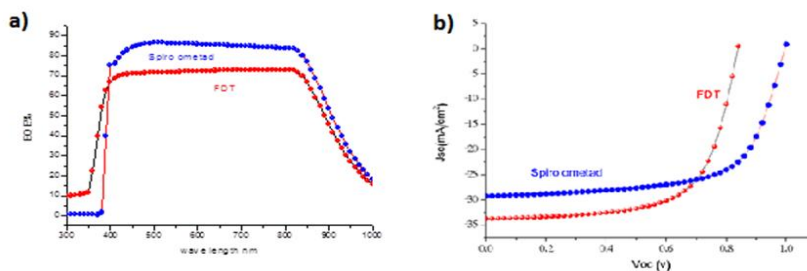


Figure 8 :The plots (a) J/V and (b) EQE

IV. Conclusion and outlook

The exceptional performance of the perovskite solar cell in terms of efficiency gives great hope for the development of photovoltaic solar energy. However, the cost of the perovskite cell darkens this hope because the spiroometad compound which is associated with the cell is very expensive. The displayed objective is to orient oneself for replacement of spiroometad. The synthesis of FDT molecule derived from spiroometad presents itself as the alternative candidate. In addition, it is cheaper and displays almost the same performance as the spiroometad. Besides the cost and efficiency problems remains that of the long-term stability of the perovskite cell. Research is carried out by everyone in photovoltaics in order to create the perovskite cell which will have the golden triangle of solar cell, namely: better efficiency; low cost and good stability over time. The energy transition will therefore have a sustainable and efficient solution.

References

- [1]. A. Kojima, K. Teshima, Y. Shirai and T. Miyasaka, *J. Am. Chem.Soc.*, 2009, 131, 6050-6055. Organometal halide perovskites as visible-light sensitizers for photovoltaic cells. doi: 10.1021/ja809598r.
- [2]. <https://www.nrel.gov/pv/assets/pdfs/best-research-cellefficiencies.20190802.pdf>
- [3]. Suneth C. Waththage in *Perovskite Photovoltaics, 2018' Evolution of Perovskite Solar Cells'* <https://doi.org/10.1016/B978-0-12-812915-9.00003-4>
- [4]. Popov, V. A. *The Akhmatov Mine in the South Urals: Notes on Mineralogy. Mineral. Alm.* 2012, 17, 8.
- [5]. B. Cai, Y. Xing, Z. Yang, W.-H. Zhang and J. Qiu, *Energy Environ. Sci.*, 2013, 6, 1480-1485.
- [6]. S. Pang, H. Hu, J. Zhang, S. Lv, Y. Yu, F. Wei, T. Qin, H. Xu, Z. Liu and G. Cui, *Chem. Mater.*, 2014, 26, 1485-1491.
- [7]. Kumar M H, Dharani S, Leong W L, Boix P P, Prabhakar R R, Baikie T, Shi C, 2014 *Adv. Mater.* 26 712
- [8]. K. D. Karlin, *Synthesis, Structure, and Properties of Organic- Inorganic Perovskites and Related Materials*, John Wiley & Sons, Inc., 2007.
- [9]. T. Baikie, Y. Fang, J. M. Kadro, M. Schreyer, F. Wei, S. G. Mhaisalkar, M. Graetzel and T. J. White, *J. Mater. Chem. A*, 2013, 1, 5628.
- [10]. J. S. Manser and P. V. Kamat, *Nat. Photon.*, 2014, 8, 737-743.
- [11]. S. D. Stranks, G. E. Eperon, G. Grancini, C. Menelaou, M. J. Alcocer, T. Leijtens, L. M. Herz, A. Petrozza and H. J. Snaith, *Science*, 2013, 342, 341-344.
- [12]. V. D'Innocenzo, G. Grancini, M. J. Alcocer, A. R. Kandada, S. D. Stranks, M. M. Lee, G. Lanzani, H. J. Snaith and A. Petrozza, *Nat. Commun.*, 2014, 5, 3586
- [13]. Abhishek Swarnkar, A. R. Marshall, E. M. Sanehira, D. T. M. Boris D. Chernomordik and J. M. L. Jeffrey A. Christians, Tamoghna Chakrabarti, *Science* (80-), 2016, 354, 92-95
- [14]. J. A. Christians, R. C. M. Fung, and P. V. Kamat, "An Inorganic Hole Conductor for Organo-Lead Halide Perovskite Solar Cells. Improved Hole Conductivity with Copper Iodide," *J. Am. Chem. Soc.*, vol. 136, no. 2, pp. 758-764, Jan. 2014.
- [15]. S. Chavhan, O. Miguel, H.-J. Grande, V. Gonzalez-Pedro, R. S. Sánchez, E. M. Barea, I. Mora-Seró, and R. Tena-Zaera, "Organometal halide perovskite-based solar cells with CuSCN as the inorganic hole selective contact," *J. Mater. Chem. A*, vol. 2, no. 32, pp. 12754-12760, Jun. 2014.
- [16]. J. H. Heo, S. H. Im, J. H. Noh, T. N. Mandal, C.-S. Lim, J. A. Chang, Y. H. Lee, H. Kim, A. Sarkar, M. K. Nazeeruddin, M. Gratzel, and S. I. Seok, "Efficient inorganic-organic hybrid heterojunction solar cells containing perovskite compound and polymeric hole conductors," *Nat. Photonics*, vol. 7, no. 6, pp. 486-491, May 2013.
- [17]. Zonglong Zhu, Yang Bai, Harrison Ka Hin Lee, Cheng Mu, Teng Zhang, Lixia Zhang *Adv. Funct. Mater.* 2014, 24, 7357. Polyfluorene Derivatives are High-Performance Organic Hole-Transporting Materials for Inorganic-Organic Hybrid Perovskite Solar Cells <https://doi.org/10.1002/adfm.201401557> [18] Michael Saliba, Simonetta Orlandi, Taisuke Matsui; Michael Graetzel and Mohammad Khaja Nazeeruddin A molecularly engineered hole-transporting material for efficient perovskite solar cells; DOI: 10.1038/ENERGY.2015.17
- [18]. Kasparas Rakstys, Cansu Içci and Mohammad Khaja Nazeeruddin Efficiency vs. stability: dopant-free hole transporting materials towards stabilized perovskite solar cells DOI: 10.1039/C9SC01184F (Minireview) *Chem. Sci.*, 2019, 10, 6748-6769
- [19]. T. Baikie, Y. Fang, J. M. Kadro, M. K. Schreyer, F. Wei, S. G. Mhaisalkar, M. Graetzel and T. J. White. Synthesis and crystal chemistry of the hybrid perovskite (CH₃NH₃)PbI₃ for solid state sensitised solar cell applications. *J. Mater. Chem. A* 1, 5628-5641 (2013).
- [20]. Murray, A. T. et al. Modular design of SPIRO-OMeTAD analogues as hole transport materials in solar cells. *Chem. Commun.* 51, 8935-8938 (2015).
- [21]. H. J. Snaith and M. Gratzel, *Adv. Mater.* 19, 3643 (2007). Electron and Hole Transport through Mesoporous TiO₂ Infiltrated with Spiro-MeOTAD <https://doi.org/10.1002/adma.200602085>
- [22]. Du, H.-J., Wang, W.-C. and Zhu J.-Z. (2016) Device Simulation of Lead-Free CH₃NH₃SnI₃ Perovskite Solar Cells with High Efficiency. *Chinese Physics B*, 25, Article ID: 108803. <https://doi.org/10.1088/1674-1056/25/10/108802>
- [23]. Mandadapu, U., Vedanayakam, V., Thyagarajan, K., Reddy, M.R. and Babu, B.J. (2017) Design and Simulation of High Efficiency Tin Halide Perovskite Solar Cell. *International Journal of Renewable Energy Research*, 7, 1603-1612.
- [24]. Kasparas Rakstys, Michael Saliba, Peng Gao, Paul Gratia, Egidijus Kamarauskas, Highly Efficient Perovskite Solar Cells Employing an Easily Attainable Bifluorenylidene-Based Hole-Transporting Material DOI: 10.1002/anie.201602545
- [25]. Usha Mandadapu, S. Victor Vedanayakam and K. Thyagarajan Simulation and Analysis of Lead based Perovskite Solar Cell using SCAPS-1D DOI: 10.17485/ijst/2017/v10i11/110721
- [26]. Faisal Baig, Bernabé Mari Soucase Numerical Analysis for Efficiency Enhancement of Thin Film Solar Cells DOI: 10.4995/Thesis/10251/118801
- [27]. Takashi Minemoto, Masashi Murata Theoretical analysis on effect of band offsets in perovskite solar cells. *Solar Energy Materials & Solar Cells* 133(2015)8-14. DOI: 10.1016/j.solmat.2014.10.036
- [28]. Wisnu Ananda Electronic and EMC Laboratory External Quantum Efficiency Measurement of Solar Cell'
- [29]. Bernabé Mari Soucase, Inmaculada Guaita Pradas and Krishna R. Adhikari Numerical Simulations on Perovskite Photovoltaic Devices' <http://dx.doi.org/10.5772/61751> (2014).
- [30]. Noh JH, Im SH, Heo JH, Mandal TN, Seok SI. Chemical management for colorful, efficient, and stable inorganic-organic hybrid nanostructured solar cells. *Nano Lett* 2013;13:1764-9.

- [31]. Hirasawa M, Ishihara T, Goto T, Uchida K, Miura N. Magnetoabsorption of the lowest exciton in perovskite-type compound (CH₃NH₃)PbI₃. *Physica B* 1994;201:427–30.
- [32]. Stranks SD, Eperon GE, Grancini G, Menelaou C, Alcocer MJ, Leijtens T, et al. Electron-hole diffusion lengths exceeding 1 micrometer in an organometal trihalide perovskite absorber. *Science* 2013;342:341–4

Aboubakary coulibaly, et al. "Experimental and Numerical study of (CH₃NH₃PbI₃) MaPbI₃ thin film with fluorene- dithiophene (FDT) or spiroometad as hole transporter layer." *IOSR Journal of Applied Physics (IOSR-JAP)*, 12(2), 2020, pp. 17-26.